




# Polyacrylonitrile modified partially reduced graphene oxide composites for the extraction of Hg(II) ions from polluted water

Fathi S. Awad<sup>1,2,\*</sup> , Khaled M. AbouZied<sup>1</sup>, Ayyob M. Bakry<sup>1,3</sup>, Weam M. Abou El-Maaty<sup>2</sup>, Ahmad M. El-Wakil<sup>2</sup>, and M. Samy El-Shall<sup>1,\*</sup>

<sup>1</sup>Department of Chemistry, Virginia Commonwealth University, Richmond, VA 23284, USA

<sup>2</sup>Chemistry Department, Faculty of Science, Mansoura University, Mansoura 35516, Egypt

<sup>3</sup>Department of Chemistry, Faculty of Science, Jazan University, Jazan 45142, Saudi Arabia

Received: 3 September 2020

Accepted: 8 January 2021

Published online:

1 February 2021

© The Author(s), under exclusive licence to Springer Science+Business Media, LLC part of Springer Nature 2021

## ABSTRACT

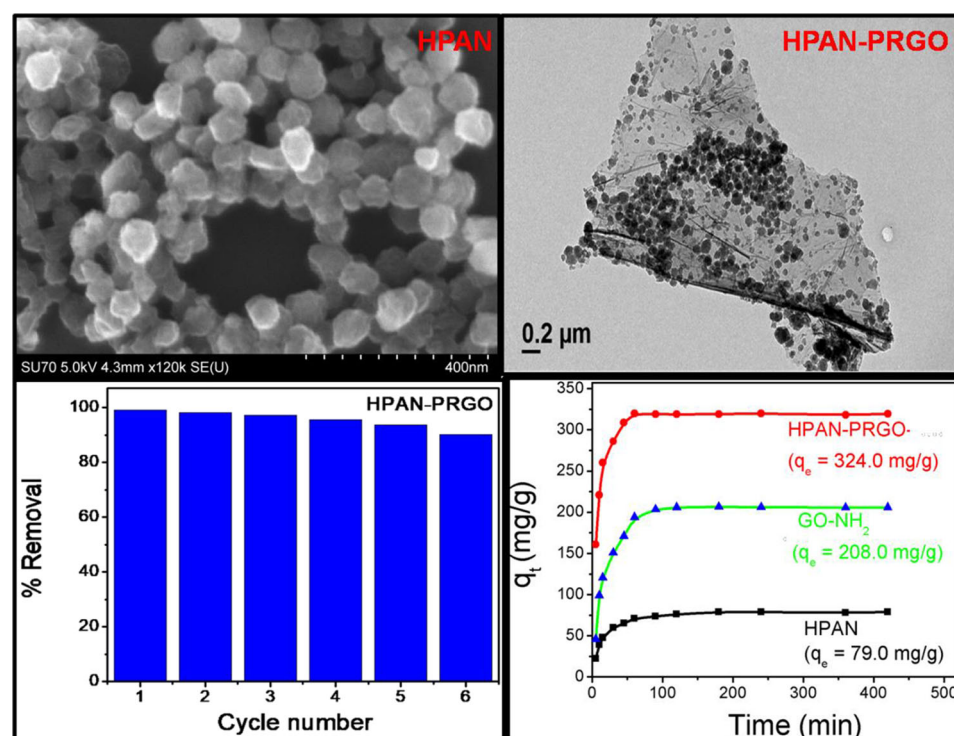
Polyacrylonitrile nanoparticles grafted on ethylene diamine functionalized partially reduced graphene oxide (PAN-PRGO) was prepared via in situ emulsion polymerization and was further modified to contain amidoxime, amidinoethylene diamine, and carboxylic groups on the surface of the graphene nanosheets via partial hydrolysis of the nitrile groups on the polymer chains of the composite using (4% NaOH, 20 min) (HPAN-PRGO). The properties and morphologies of the prepared composites were compared through FTIR, UV–Vis, Raman spectra, XRD, SEM, TEM, and XPS analysis. The results revealed that polyacrylonitrile nanoparticles were grafted on the surface of the aminated graphene oxide nanosheets via the reaction between the free amino groups of the ethylene diamine modified graphene oxide nanosheets and nitrile groups of acrylonitrile (AN). The obtained HPAN-PRGO composite was evaluated for its chelating property with Hg(II) ions. The effect of initial pH, initial concentration of the Hg(II), adsorbent dose, and contact time on the extraction of Hg(II) ions using HPAN-PRGO were investigated. The adsorption experiments indicated that HPAN-PRGO exhibits higher affinity toward Hg(II). The maximum uptake capacity for the extraction of Hg(II) ions on HPAN-PRGO was 324.0 mg/g at pH 5. The HPAN-PRGO shows a 100% removal of Hg(II) at concentrations up to 50 ppm, and the adsorption is exceptionally rapid showing more than 80.0% removal within 15 min and 100.0% of  $q_e$  within 1.5 h at 800 ppm concentration. The Langmuir isotherm model and pseudo-second-order kinetic model have showed good fitness with the practical data. The XPS analysis of HPAN-PRGO before and after adsorption revealed the chelation adsorption mechanism between mercury and amine, amide, amidoxime, and carboxylic

Handling Editor: Chris Cornelius.

Address correspondence to E-mail: fathyawad949@gmail.com; mselshal@vcu.edu

groups. After six adsorption–desorption cycles, the HPAN-PRGO could retain more than 90.0% of its original adsorption capacity. These results confirmed that HPAN-PRGO has exceptional performance for the removal of Hg(II) from wastewater.

## GRAPHICAL ABSTRACT



## Introduction

In recent years, water pollution by highly toxic heavy metals is a serious worldwide problem [1, 2]. Among many heavy metal ions, mercury, in particular, is recognized as one of the most harmful contaminants in the environment on account of its high volatility, bioaccumulation, and toxicity [3]. Exposure to mercury causes severe damage to lungs, kidneys, brain and other organs [4, 5]. Mercury is often released (discharged) to the environment through industrial wastewaters, electroplating and batteries, mining activities, fertilizers, and pharmaceuticals [6]. Methyl mercury is more toxic than other mercury species; however, it is feasible to be transform mercury to

methyl mercury through both a biotic and biotic methylation processes after being released to the environment [6–9]. Most of mercury in wastewater exists in the form of mercury ions. Thus, to protect ecosystems, the discharge of Hg(II) is under strict regulatory limits, and the permissible concentration limit of mercury in drinking water is 2 ppb according to the United States Environmental Protection Agency (EPA) [10]. Until now, various techniques have been utilized to extract/reduce Hg(II) ions from aquatic solutions such as precipitation, adsorption, membrane process, chemical coagulation, and ion exchange [1, 11]. Among various traditional techniques for mercury removal, adsorption is regarded as an effective, easy, and economic method to purify water. Various adsorbents such as activated carbons

[12], carbon nanotubes [13], modified mesoporous silica [14], Mg<sub>2</sub>Al layered double hydroxide [15], polymers [16, 17], graphene oxide [18–20], natural zeolites [21], clay [22], and chelating materials [23] have been utilized for the heavy metal removal from contaminated water. The adsorption properties of these materials based on the presence of chelating functional group(s) on their surfaces which can coordinate with the metal ions, where it has been found that materials functionalized with nitrogen-based ligands (such as imidazole, hydrazine groups, amino, and amidoxime groups) shown high binding affinity to mercury [1, 24, 25]. Aliphatic polymers containing nitrogen functional groups have been utilized for water purification, but their surface area is small. However, carbon and carbon-based derivatives-polymeric composites have revealed high efficiency for the extraction of mercury and toxic heavy metals from wastewater.

Among these carbon materials, graphene oxide (GO) [26] is a single atom thick two-dimensional graphitic carbon and its surface has reactive oxygen functional groups which facilitates the covalent bonding with other functional groups. Graphene has extra ordinary thermal, mechanical, and electrical properties, high surface area (2630 m<sup>2</sup>g<sup>-1</sup>) and tailorable functionalities [27]. During the past few years, functionalization of graphene with polymers having chelating groups has gained great attention to enhance the adsorption properties of graphene. Chandra and Kim prepared polypyrrole-reduced graphene oxide composite with high capacity and selectivity for mercury (II) based on the functional groups of the polypyrrole [28]. The covalently linked hybrid structure can bring about outstanding physiochemical stability. There are still no reports on the development of polymer-grafted RGO hybrids. The present study was intended to develop a new hybrid polyacrylonitrile (PAN)-grafted ethylene diamine partially reduced graphene oxide (GO-NH<sub>2</sub>). Polyacrylonitrile was selected as a promising polymer for the development of PRGO composite due to the unique properties of PAN such as non-toxicity, excellent environment stability, ease of preparation, and low cost with good physical properties such as hardness and high chemical resistance. Also, polyacrylonitrile contains pendant nitrile (CN) functional groups so it can be easily chemically modified to amidoxime (AO) groups, which have high affinity to coordinate with metal ions [29, 30]. The high surface

area of partially reduced graphene oxide (RGO) and the high stability and non-toxicity of polyacrylonitrile motivated the preparation of PAN-PRGO composite for Hg (II) extraction from wastewater.

In this work, a novel route to prepare PAN nanoparticles covalently grafted on the surface of functionalized GO nanosheets is introduced. The preparation is accomplished via chemical oxidation of graphite to graphene oxide (GO) and then functionalized with ethylene diamine followed by reaction between nitrile group of acrylonitrile (AN) and free amino group on the surface of functionalized Go during the emulsion polymerization of AN, thereby yielding highly covalently attached PAN-PRGO. After that, the free nitrile groups on the polymer chains of the composite undergo partial hydrolysis (using 20.0% NaOH for 20 min) to amide, amidoxime and carboxylate groups which promote the capacity of graphene for the extraction of mercury (II) ions. The general procedure for the preparation of HPAN-PRGO is shown in Scheme 1.

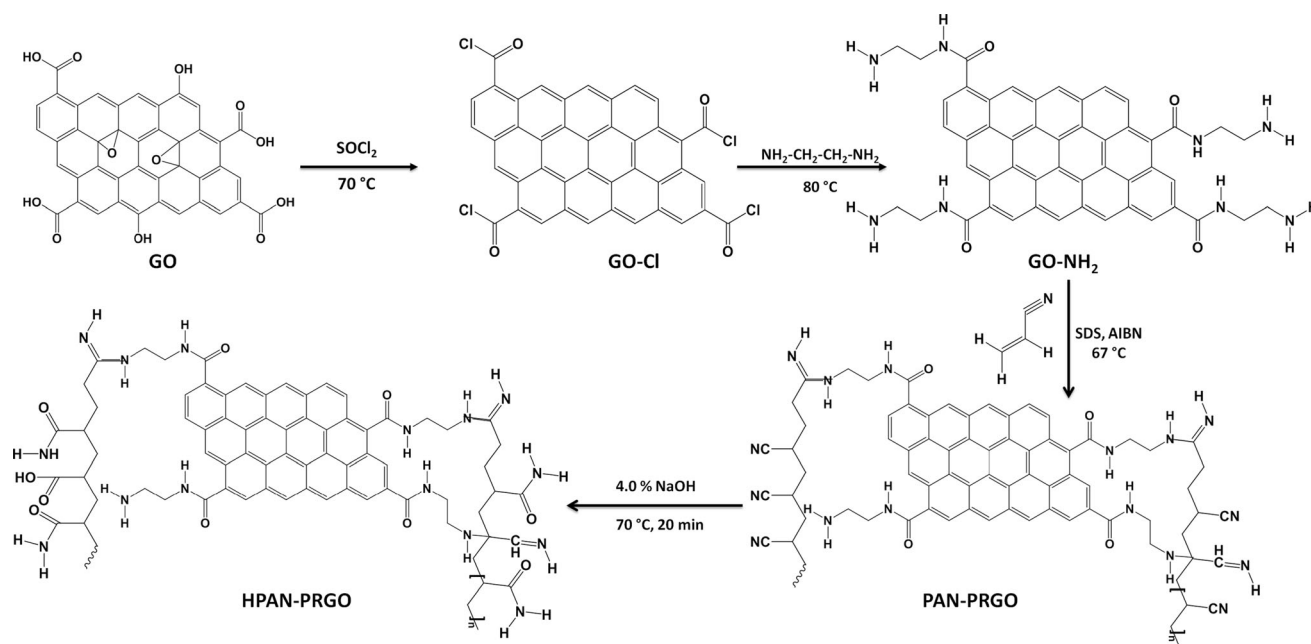
## Experimental section

### Materials

Natural graphite flakes (99.9999%), potassium permanganate (99.0%), sulphuric acid (98.0%), hydrogen peroxide (35.0%), phosphoric acid (85.0%), acrylonitrile (99.0%), ethylene diamine (99.0%), sodium dodecyl sulfate (SDS) (99.0%), azo-bis-isobutyronitrile (98.0%), and ethylenediaminetetraacetic acid (EDTA) (98.0%) were purchased from sigma and used without further purification. Mercuric chloride was used as a precursor for Hg(II) ions. Deionized (DI) water was used throughout these experiments.

### Synthesis of polyacrylonitrile/partially reduced graphene oxide nanocomposite (PAN-PRGO)

0.5 g of NH<sub>2</sub> terminated graphene oxide, prepared via the improved Hummer method [19, 31] and our previous work [20], 0.4 g of SDS and 120 mL deionized water were put into a three-necked round-bottomed flask. The mixture was sonicated for 30 min and stirred for 30 min to produce micelles. The suspension was then heated to 69°C and kept at that temperature. 0.150 g of AIBN (dissolved in 1.0 mL of DMF) was injected. After 15 min, 10 mL of



**Scheme 1** General steps for the synthesis of hydrolyzed polyacrylonitrile/partially reduced graphene oxide nanocomposite (HPAN-PRGO).

acrylonitrile monomer was added. After that, the reaction was allowed to occur for 5 h under nitrogen protection and constant stirring. Finally, the PAN-PRGO nanocomposite was centrifuged and washed with excess ethanol and deionized water to remove unreacted monomer then dried overnight at 70 °C.

### Synthesis of hydrolyzed polyacrylonitrile nanoparticles (HPAN) and hydrolyzed polyacrylonitrile/partially reduced graphene oxide nanocomposite (HPAN-PRGO)

0.21 g of PAN nanoparticles, prepared via Zhao et al method [32], or PAN-PRGO were introduced into 4 ml NaOH (4%) solution in 50 mL a round-bottomed flask and refluxed at 70 °C for 20 min. Finally, the mixture was filtered and washed with diluted HCl and deionized water until pH 7.5 then dried under vacuum at 70 °C. General steps for the synthesis of hydrolyzed polyacrylonitrile/ $\text{NH}_2$ -terminated graphene oxide nanocomposite (HPAN-PRGO) are shown in Scheme 1.

### Mercury (II) adsorption onto PAN, HPAN, GO, GO- $\text{NH}_2$ , and HPAN-PRGO adsorbents

The adsorption capacities of the prepared adsorbents toward mercury(II) were evaluated by batch

adsorption experiments, and the effects of several parameters, such as pH value of the solution, adsorbent dose, initial concentration of Hg(II), and contact time have been investigated.

**Adsorption isotherm** Equilibrium studies of mercury species were evaluated by varying the initial mercury concentration (5–1000 mg/L) at pH 5. 0.01 g of the adsorbent was mixed with 10.0 mL of Hg(II) solution at various initial concentrations and stirred for 2 h on a shaker to reach the adsorption equilibrium. The final mercury concentration was measured by ICP-OES.

The adsorption capacity and the percent of removal (% R) were determined from the following equations.

$$\% R = \frac{(C_0 - C_e)}{C_0} \times 100 \quad (1)$$

$$q_e = \frac{(C_0 - C_e)V}{m} \quad (2)$$

where  $C_e$  and  $C_0$  (mg/L) are the liquid phase concentration of heavy metal ions at equilibrium and initial, respectively,  $m$  is the mass of adsorbent (g), and  $V$  (L) is the volume of testing solution of heavy metal ions.



### Effect of dosage and pH

The effect of adsorbent dose on the Hg(II) extraction using HPAN, IGO-NH<sub>2</sub>, and HPAN-PRGO was performed by adding ( 5, 10, 15, 20, 30, 30 mg ) in a 20 ml glass vial containing 10 ml of mercury(II) in certain concentration. At the adsorbent dose, (1 g/L) the effect of pH was determined by varying solution pH (1–6) by adding few drops of 0.01 M NaOH and 0.01 M HCl solution. The experiments were conducted under continuous magnetic agitation for 120 min at 25 °C. After that, the sample was separated, and the equilibrium concentration of mercury (II) was measured using ICP-OES.

### Adsorption kinetic study

Adsorption kinetic experiments for Hg(II) under various adsorption times (5–420 min) were performed. For each operation, 10 mg of solid adsorbent was weighted into a glass vial, and a 10 mL aqueous solution of mercury of definite concentration was added. These solutions were conditioned to a pH of 5 and stirred for varying time periods from 5 to 420 min at room temperature. At specific time intervals, the suspensions were centrifuged, and the equilibrium concentration of Hg (II) were measured by ICP-OES. The practical data obtained were described by the pseudo-second-order and pseudo-first-order as shown in Table 2.

### Desorption–regeneration cycles

Six adsorption–desorption–regeneration cycles were carried out to evaluate the sustainability of the HPAN-PRGO adsorbent. Before desorption, adsorption experiments were conducted by adding 10 mg of each material into a solution containing 800 mg/L of Hg(II) and stirred for 2 h. The mixture then centrifuged and the concentration of mercury in the supernatant was measured by ICP-OES. The Hg-loaded adsorbents were then washed and dried at 80 °C.

**For desorption**, 0.01 g of Hg-loaded HPAN-PRGO added to 10 mL of the eluent solution (2.0 M HCl or 0.017 M EDTA) and agitated for 4 h. The suspension was then centrifuged, and the concentration of mercury (II) in the supernatant was determined using ICP-OES. The desorption efficiency was determined via Eq.(3) .

$$\% \text{ Desorption Efficiency} = \frac{(C_e - C_0)V_e}{q_e m} \times 100 \quad (3)$$

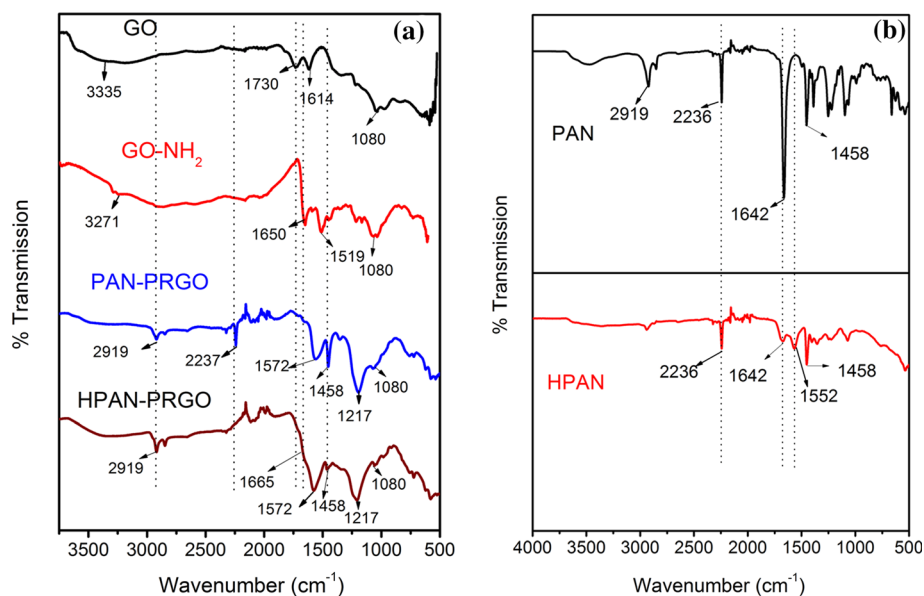
where  $q_e$  is the adsorption capacity in the removal test and  $m$  is the mass of HPAN-PRGO adsorbent,  $V_e$  is the volume of the eluent (L),  $C_0$  is the initial concentration of heavy metal ions in the eluent (mg/L), and  $C_e$  is the equilibrium concentration (mg/L) after desorption.

## Results and discussion

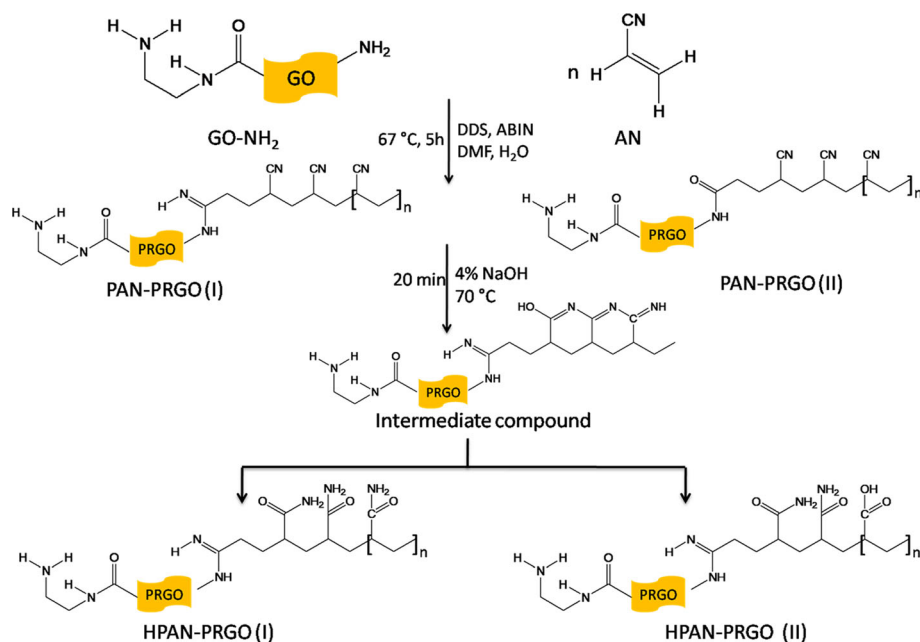
### Characterization of PAN, HPAN, GO, GO-NH<sub>2</sub>, PAN-PRGO, and HPAN-PRGO

To confirm the formation of GO, GO-NH<sub>2</sub>, PAN, PAN-PRGO, HPAN, and HPAN-PRGO composite, FTIR spectra were collected and presented in Fig1a and b. The FTIR spectrum of GO reveals different types of oxygen containing functional groups such as a peak at 1730 cm<sup>-1</sup> for C=O moiety of COOH groups and a broad peak at 3335 cm<sup>-1</sup> due to O–H stretching vibration of hydroxyl groups [19]. The peaks at 1080 cm<sup>-1</sup> and 1156 cm<sup>-1</sup> are ascribed to alkoxy and epoxy stretching, respectively [19, 20]. The ethylene diamine modified graphene oxide displayed a characteristic new peak at 3271 cm<sup>-1</sup> corresponding to the N–H stretching of primary amines and a sharp peak at 1650, attributed to the N–H bending of O=C–NH<sub>2</sub> or NH<sub>2</sub> [19, 20]. These results indicate the successful functionalization of GO with ethylene diamine through the amine group and the amide linkage. The FTIR spectra of pure PAN display characteristic peaks at 2236 cm<sup>-1</sup> for the stretching vibration of CN and at 2919 cm<sup>-1</sup> and 1458 cm<sup>-1</sup> for the stretching and bending vibrations of CH<sub>2</sub> [33, 34]. The peak at 1642 cm<sup>-1</sup> confirms the presence of CN group. The FTIR spectrum of PAN-PRGO shows a peak at 2237 cm<sup>-1</sup> nitrile group (CN) and a peak at 2919 cm<sup>-1</sup> for the stretching vibration of CH<sub>2</sub> as in pure PAN. Moreover, the peak at 3271 cm<sup>-1</sup> and 1650 cm<sup>-1</sup> of GO–NH<sub>2</sub> reduced or completely disappeared and a new peak appeared at 1572 cm<sup>-1</sup> due to amide group (C=O–NH<sub>2</sub>) or the amidine group (N–C=N) indicating the reaction between the free amino group of ethylene diamine modified graphene oxide with the nitrile group of AN to form –NH–CO– or (N–C=N) [1, 35, 36] as shown in Scheme 2. Additionally, the peaks at 1458

**Figure 1** FTIR for **a** GO, GO-NH<sub>2</sub>, PAN-PRGO, and HPAN-PRGO. **b** PAN, and HPAN.



**Scheme 2** Represent the mechanism of the reaction between aminated graphene oxide and acrylonitrile.



and  $1217\text{ cm}^{-1}$  may be due to the formation of  $\text{-NH-C=N-CH}_2$ . Figure 1b reveals the FTIR spectra of partial alkaline hydrolysis of PAN using 4% NaOH. It revealed that the peak at  $2237\text{ cm}^{-1}$  reduced after hydrolysis, while the stretching bands of C=O and NH<sub>2</sub> in amide groups were observed at  $1665\text{ cm}^{-1}$  and  $1572\text{ cm}^{-1}$ . The FTIR spectrum of HPAN-PRGO showed that the peak at  $2237\text{ cm}^{-1}$  of CN group disappeared entirely; moreover, it showed two peaks overlapped at  $1665$  and  $1572$  attributed to N-H group and COONa. Two new peaks at  $1572$  (C=O) and  $1665\text{ cm}^{-1}$  ( $\text{-NH}_2$ ) appeared confirming that the

hydrolysis reaction is done [34, 36]. The spectrum also showed that the peak of epoxy group at  $1080\text{ cm}^{-1}$  decreased indicating that the GO is partially reduced. These results clearly confirmed that aminated graphene oxide was successfully formed and acrylonitrile (AN) was simultaneously grafted and polymerized at the NH<sub>2</sub> group of IGO-NH<sub>2</sub> during the polymerization resulting in covalently hybrid structured (HPAN-PRGO). According to the FTIR results, the mechanism of the reaction between GO-NH<sub>2</sub> and acrylonitrile can be suggested as Scheme 2.

**Figure 2** **a** XRD patterns of GO, GO-NH<sub>2</sub>, HPAN, and HPAN-PRGO **b** Raman spectra of HPAN-PRGO, GO, HPAN, and GO-NH<sub>2</sub>.

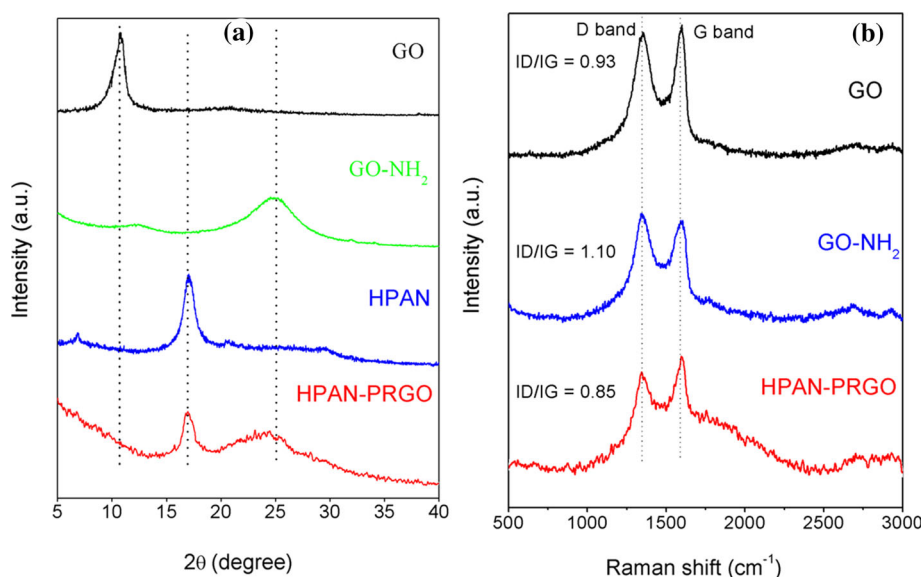


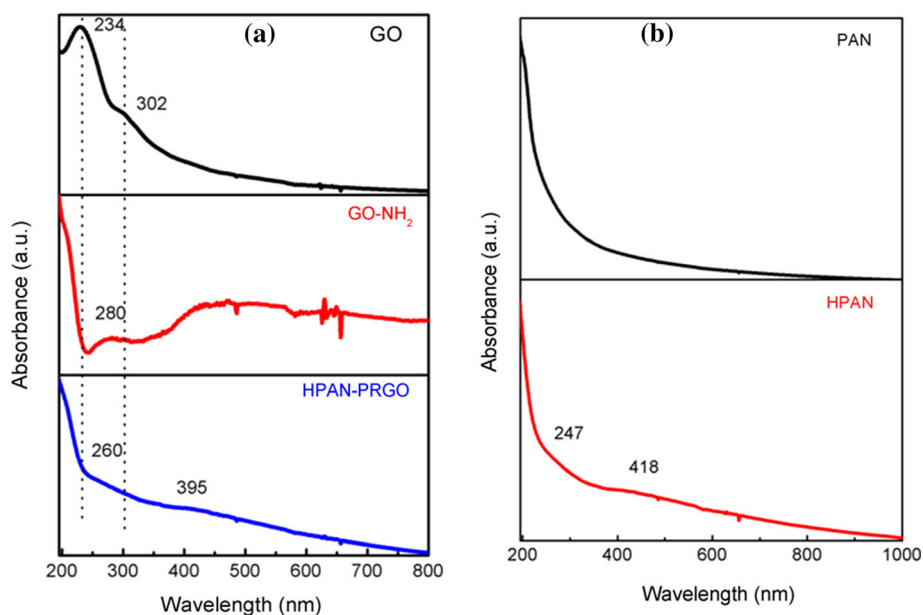
Figure 2a displayed the X-ray diffraction patterns of GO, GO-NH<sub>2</sub>, HPAN, and HPAN-PRGO. For the GO synthesized by the chemical oxidation of graphite, the presence of a peak at  $2\theta = 10.93$  is related to the oxygen containing functional groups on the GO sheets [37, 38]. On chemical modification with ethylene diamine, the sharp peak of GO faded and a broad peak at  $2\theta = 24.9$  appeared indicating that the graphene oxide may be partially reduced and also may be due to the restacking of the aminated graphene oxide nanosheets [26]. For the HPAN, the spectrum shows a diffraction peak at  $2\theta = 17.35$  corresponds to the (100) crystallographic planes of PAN (due to PAN intermolecular spacing) due to the intermolecular repulsion of the nitrile dipoles [35, 39]. For HPAN-PRGO, the spectrum also shows a weak reflection peak at  $2\theta = 16.91$  which can be ascribed to the (100) crystal planes of polyacrylonitrile suggesting that GO supports the formation of the PAN nanoparticles. After grafting of HPAN on the aminated graphene oxide nanosheets, the intensity of the reflection peak of PAN decreased obviously, indicating a decrease in the polar interaction between the molecular chains and the breakage of bonds in the inner crystal region during the reaction between the free NH<sub>2</sub> on the surface of GO and the nitrile group of PAN.

Figure 2b shows the Raman spectra of the GO, GO-NH<sub>2</sub>, and HPAN-PRGO composite with two characteristic G and D bands. The G-band is associated with the vibration of the sp<sup>2</sup>-hybridized carbon to sp<sup>3</sup>-hybridized carbon originating from the

demolition of the sp<sup>2</sup> structures of the graphite or covalent attachment of functional groups and it appears at 1592 cm<sup>-1</sup> in IGO and with a blue shift in GO-NH<sub>2</sub> (1598 cm<sup>-1</sup>) and HPAN-PRGO (1605 cm<sup>-1</sup>) which could be due to charge transfer from the nitrile group of the HPAN to the aminated graphene oxide nanosheets. The intensity ratio of the D-band to the G-band is used to evaluate the quality of the graphitic structures because for highly ordered pyrolytic graphite, this ratio approaches zero as a measure of the degree of disorder and defects in the graphitic structure. The I<sub>D</sub>/I<sub>G</sub> in the GO-NH<sub>2</sub> (1.1) is slightly higher than that of IGO (0.93) indicating a small increase in the disorder structure due to covalent interaction of ethylene diamine with the GO nanosheets [40]. For HPAN-PRGO, the spectrum shows enhanced intensity for the G-band with blue shift. In addition, the I<sub>D</sub>/I<sub>G</sub> in the HPAN-PRGO (0.85) is slightly lower than that of GO confirming the interaction between the CN group of HPAN and the free NH<sub>2</sub> group on the GO nanosheets [28].

Figure 3a and b display the UV-Vis absorption spectra of the GO-NH<sub>2</sub>, GO, HPAN-PRGO, PAN, and HPAN nanoparticles dispersed in water. The UV-Vis spectra of GO reveal a shoulder-like absorption peak appeared at 302 nm owing to the n-π\* transitions of the C-O, C=O bonds and a strong peak at 234 nm, corresponding to the π-π\* of the C=C in GO. On chemical modification with ethylene diamine, the red shift of the π-π\* transitions indicates the partial reduction of GO [40, 41]. For the HPAN UV-Vis spectra, it is clear that the HPAN nanoparticles

**Figure 3** UV–Vis spectra of **a** GO, GO-NH<sub>2</sub> and HPAN-PRGO composite. **b** PAN, and HPAN nanoparticles.



had absorption enhancement in the UV region (200–400) with a peak at 247 nm and 395 nm compared to that of the PAN nanoparticles. This 247 nm band peak represented a  $\pi$ - $\pi^*$  transition of the C=N and C=O, whereas the peak at 395 nm may be corresponding to the  $n$ - $\pi^*$  transitions of C=O and C=N. For the HPAN-PRGO, the red shift of the  $\pi$ - $\pi^*$  transition of the aromatic C=C bond to 260 nm and the red shift of  $n$ - $\pi^*$  transition of C=N, C=O, C-O, and C-N to 395 nm indicates the interaction between CN group of PAN and GO nanosheets followed by hydrolysis of the remainder CN groups.

At last, PAN nanoparticles (latexes) were grafted on the surface of aminated graphene nanosheets via

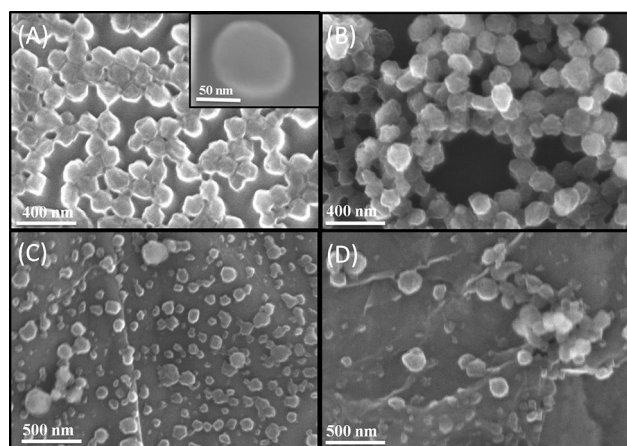


**Figure 4** SEM images of **a** PAN, **b** HPAN, **c** PAN-PRGO, **d** HPAN-PRGO.

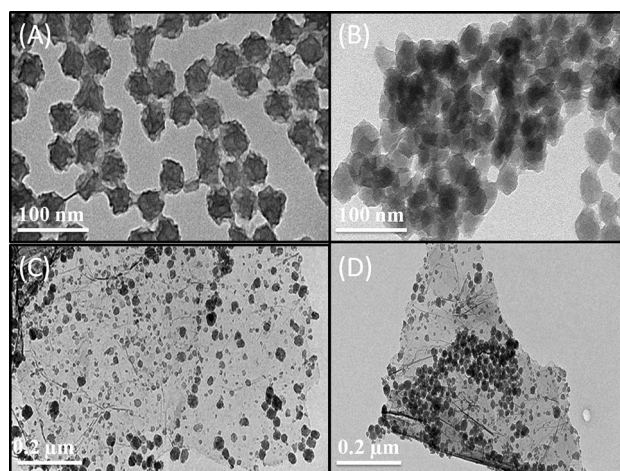


**Figure 5** TEM images of **a** PAN, **b** HPAN, **c** PAN-PRGO, **d** HPAN-PRGO.

in situ emulsion polymerization. The morphologies of the PAN, HPAN, PAN-PRGO, and HPAN-PRGO were characterized by SEM and TEM. As shown in Figs. 4 and 5, the TEM and SEM images of PAN-PRGO and HPAN-PRGO composite show graphene sheets covered homogeneously with PAN nanoparticles suggesting the growth of PAN nanoparticles along graphene sheets. Therefore, PAN could be polymerized (grafted) on the amine functionalized graphene oxide nanosheets. The PAN and HPAN nanoparticles had a narrow size distribution, largely in the range of 40–60 nm as described by SEM. Furthermore, the high magnification of the SEM image shows that the PAN latex was composed of spherical



particles with sharp edges. Compared with PAN, the HPAN particles revealed an increase in diameter corresponding to the hydrolysis of CN groups to COOH and CONH<sub>2</sub> on the polymer chains without significant change on their overall morphology [34]. The majority of the latexes are still composed of spherical particles; nevertheless, there was evidence of adjacent latex conglomerating to each other at touching points due to crosslinking or hydrolysis.

The grafting of PAN nanoparticles onto the surface of aminated graphene nanosheets was confirmed by X-ray photon spectroscopy shown in Figs. 6 and 1S. In the XPS survey spectra shown in Fig. 1S (Supporting Information). The intensity of the peak

related to C 1s enhanced significantly from GO and GO-NH<sub>2</sub> to HPAN-PRGO, while the oxygen peak decreased from GO to GO-NH<sub>2</sub> and increased again from GO-NH<sub>2</sub> to HPAN-PRGO. Additionally, the GO-NH<sub>2</sub> and HPAN-PRGO samples also clearly show the N 1s peak. The intensity of the N 1s peak increased from GO-NH<sub>2</sub> to HPAN-PRGO. These observations confirmed that aminated graphene oxide was successfully formed and acrylonitrile (AN) was simultaneously grafted polymerized at the NH<sub>2</sub> group of NH<sub>2</sub>-IGO during the polymerization resulting in covalently hybrid structured (HPAN-PRGO). The C 1s high resolution spectrum (Fig. 6a) attributed to the GO was deconvoluted to three peaks

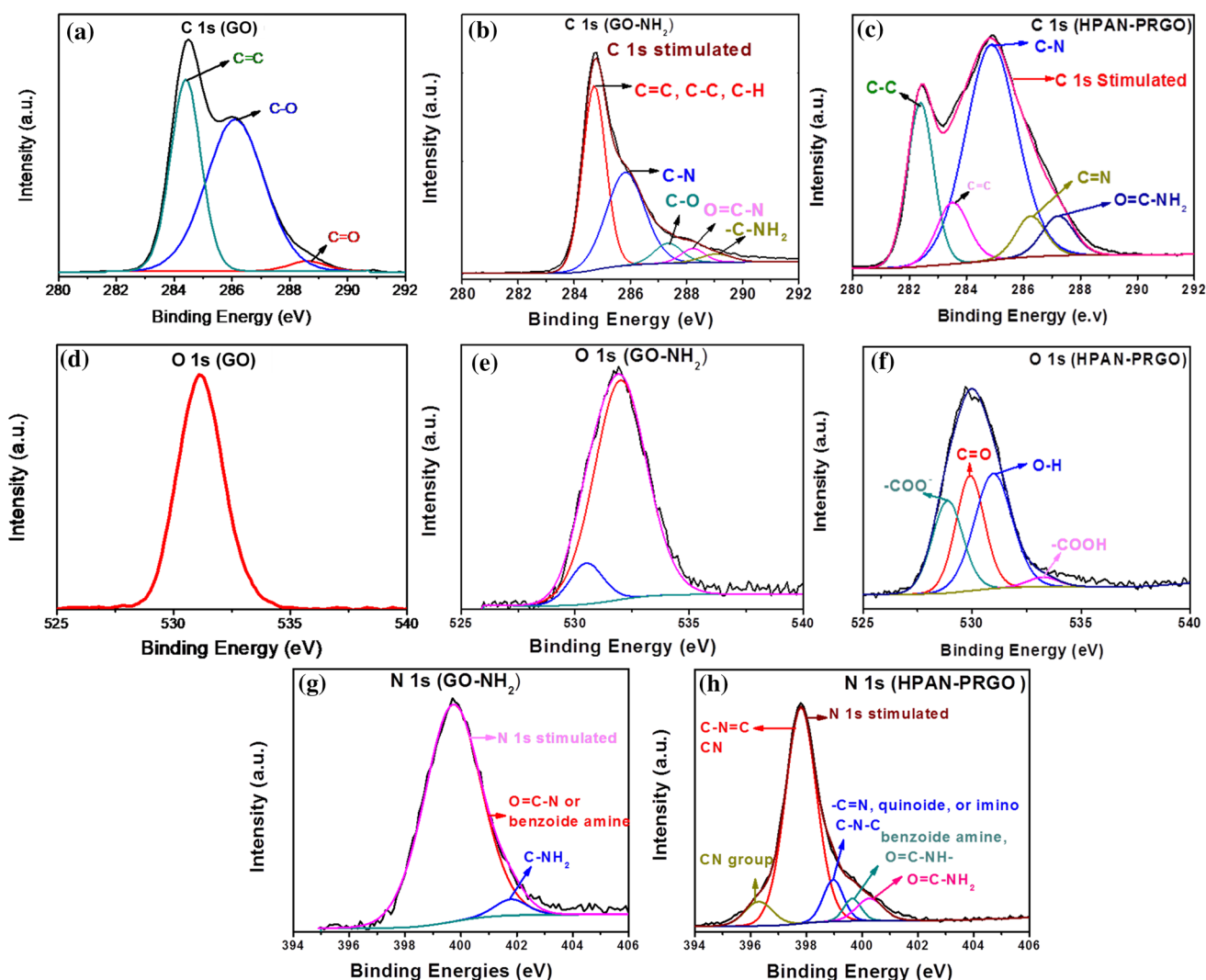


**Figure 6** The XPS spectra of C1s in GO, GO-NH<sub>2</sub>, HPAN-PRGO (a,b,c), XPS spectra of O 1s of GO, GO-NH<sub>2</sub>, HPAN-PRGO (d,e,f) and XPS spectra of N 1s of GO-NH<sub>2</sub>, and HPAN-PRGO (g,h).

with binding energies about 284.7 (C in C–H, C=C), 288.3 (C in C=O), 286.2 (C in C–O) [42]. The high resolution (Figure 6b) related to IGO–NH<sub>2</sub> was deconvoluted to five peaks with binding energies about 284.7 (C in C–H, C=C, C–C), 298.2 (C in C–NH<sub>2</sub>), 285.8 (C in C–N), 287.4 (C in N–C=O). So, the chemical modification with ethylene diamine was confirmed by the peaks at 285.8 (C–N), C–NH<sub>2</sub>, and O=C–NH<sub>2</sub>). The C 1s high resolution spectrum related to the HPAN-PRGO (Fig. 6c) was deconvoluted to five peaks with binding energies 283.8 (C in C=C, C–H), 283.1 (C in C–C), 286.4 (C in C=N, CN), 285.1 (C in C–N), and 287.3 (C in N–C=O), so the reaction between the CN group of PAN and the free NH<sub>2</sub> group on the graphene nanosheets was confirmed by the disappearance of a peak at 289.2 (C in C–NH<sub>2</sub>) in GO–NH<sub>2</sub> and the appearance of a peak at 286.4 (C in C=N, CN) [43]. The existence of N 1s peak and O 1s peak in the survey spectra of HPAN-PRGO confirmed the successful grafting of AN on graphene sheets. The high resolution of N 1s peak (Fig. 6g) related to GO–NH<sub>2</sub> can be deconvoluted into two peaks 399.8 (N in O=NH–) and 401.8 (N in NH<sub>2</sub>). The high resolution oxygen O 1s peak related to GO–NH<sub>2</sub> can be deconvoluted to two peaks at 530.7 and 532.1 related to O in O=C–NH). The high resolution of N 1s peak (Fig. 6h) related to HPAN–PRGO–NH<sub>2</sub> can be deconvoluted into five peaks 396.4, 397.6 (N in CN), 399.0 (N in C=N), 397.6 (N in O=C–NH–, –N–C=N), 400.4 (N in O=C–NH<sub>2</sub>) [44, 45]. The O 1s peak related to HPAN–PRGO–NH<sub>2</sub> (Figure F) can be deconvoluted to four peaks 528.9 (O in COO<sup>–</sup>), 530 (O in OH), 531 (O in O=C), 533 (O in COOH) [43]. So, the grafting of AN on IGO–NH<sub>2</sub> was confirmed by the disappearance of peak at 401.8 of NH<sub>2</sub> and the appearance of 399 (C=N), the partial hydrolysis of PAN grafted on graphene sheets was also confirmed by the appearance of peaks at 528.9 (O in COO<sup>–</sup>) and 533 (O in COOH). These peaks were also confirmed by the XPS results of pure PAN and HPAN as shown in Figure S2 (Supporting Information). Compared with XPS survey of PAN, the HPAN XPS spectra showed O 1s peak. From the deconvolution of N 1s and O 1s of pure HPAN, the appearance of peaks at 398.7 (N in –C=N, quinoide imine), 399.7 (N in N–C=O), and 528.1, 532.9 (O in COONa, COOH) and these observations confirm the partial hydrolysis of PAN using 4% NaOH for 20 min [36, 46].

## Adsorption Performance studies

### Effect of pH on Hg(II) adsorption

The solution pH is considered as one of the most important parameters during the adsorption process. In this perspective, the experiments were conducted at various pH conditions ranged from 1 to 6 using few drops of 0.01 M HCl and 0.01 M NaOH. When the pH is more than 5.5, Hg(OH)<sub>2</sub> becomes the major species and begins to precipitate out of the solution. So, the suitable pH range was from 1 to 5. The speciation studies have confirmed that at pH < 3, the mercury is present as Hg(II), whereas at pH > 5 Hg(OH)<sub>2</sub> is the predominant species and both of these species along with HgOH<sup>+</sup> are present at pH 3–5. As presented in Fig. 7a, the removal efficiency of mercury increased from 20.0 to 52.0 %, from 29.6 to 83.9 %, and from 32.0 to 99.68 % for HPAN, GO, HPAN-PRGO, respectively as the pH of the initial solution increased from 1 to 5. This may be attributed to the lone pair of electrons of nitrogen and oxygen which can adsorb and coordinates with mercury (II) and forms a stable complex. At pH values lower than 5, the adsorption efficiency of mercury ions decreased due to the competitive adsorption between Hg(II) ions and the available H<sup>+</sup> ions. Moreover, the protonation of the primary, secondary amines and carboxylic groups (COOH<sup>+</sup>, –NH<sub>3</sub><sup>+</sup>, O=C–NH<sup>+</sup>–) increased the positive charges on the adsorbent surface resulting an increase in the electrostatic repulsion for mercury(II) ions. The decrease in the removal of mercury above pH 5.5 is related to the formation of insoluble Hg(OH)<sub>2</sub> and it keeps constant for pH higher than 5. This may be attributed to the competitive adsorption from OH<sup>–</sup> ions by the formation of the hydrogen bonding leading to a decrease in the number of available adsorption sites [10].

### Adsorption isotherms

The adsorption capacity of the adsorbents can be determined by Hg(II) adsorption at different initial concentrations as shown in Fig. 7b. From the figure, it is clear that, when the initial concentration of Hg(II) increases, the amount of Hg(II) adsorbed at equilibrium (q<sub>e</sub>) increases until maximum adsorption was reached gradually after the concentration reached 250, 600, 800 mg/L for HPAN, GO–NH<sub>2</sub> and HPAN-PRGO, respectively, which explained that there were

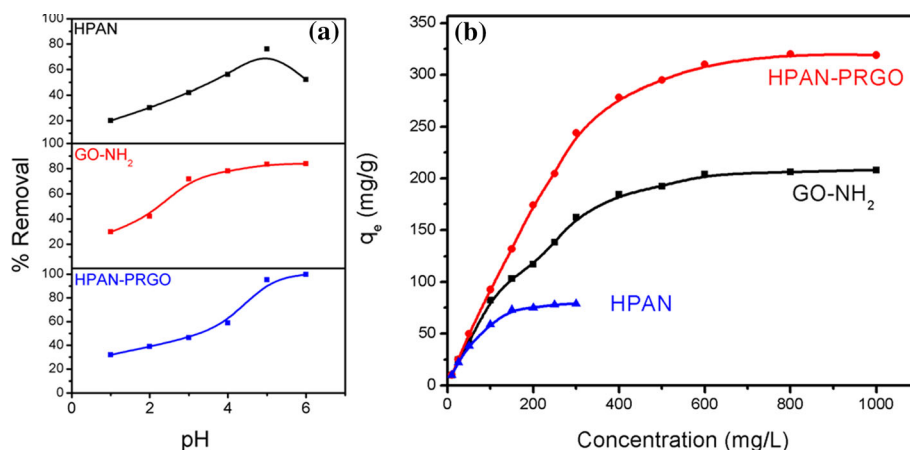


**Figure 7** **a** Effect of the solution pH on the Hg(II) removal on HPAN, GO-NH<sub>2</sub>, and HPAN-PRGO. (conditions: adsorbent dose = 0.01 g/ 10 ml, C<sub>0</sub> = 50 mg/L, T = 273 K, t = 120 min). **b** Effect of initial concentration of (Hg (II) ions) on the Hg(II)

extraction on HPAN, GO-NH<sub>2</sub>, and HPAN-PRGO. (conditions: C<sub>0</sub> = 10–1000 mg/L, T = 273 K, adsorbent dose = 0.01 g/ 10 ml, pH = 5, t = 120 min).

**Table 1** The maximum adsorption capacities of Hg(II) on GO, PAN, HPAN, GO-NH<sub>2</sub>, PAN-PRGO, and HPAN-PRGO composite

Adsorbents	q <sub>e(max)</sub> (mg/g)
GO	24.0
Pure PAN nanoparticles	28.0
HPAN nanoparticles	79.0
GO-NH <sub>2</sub>	208.0
PAN-PRGOComposite	224.0
HPAN-PRGOComposite	324.0

few available active sites on the adsorbents and suggested that the adsorption reached equilibrium. It is observed that the mercury adsorption increases in the order of HPAN-PRGO > PAN-PRGO > GO-NH<sub>2</sub> > HPAN > PAN > GO under all conditions studied such as pH (5), temperature (273 K), sorbent dose (1 g/L), and concentration, as shown in Table 1. The equilibrium data were fitted by using Freundlich and Langmuir isotherms models and the details of each isotherm model can be explored in the Supporting Information S1.

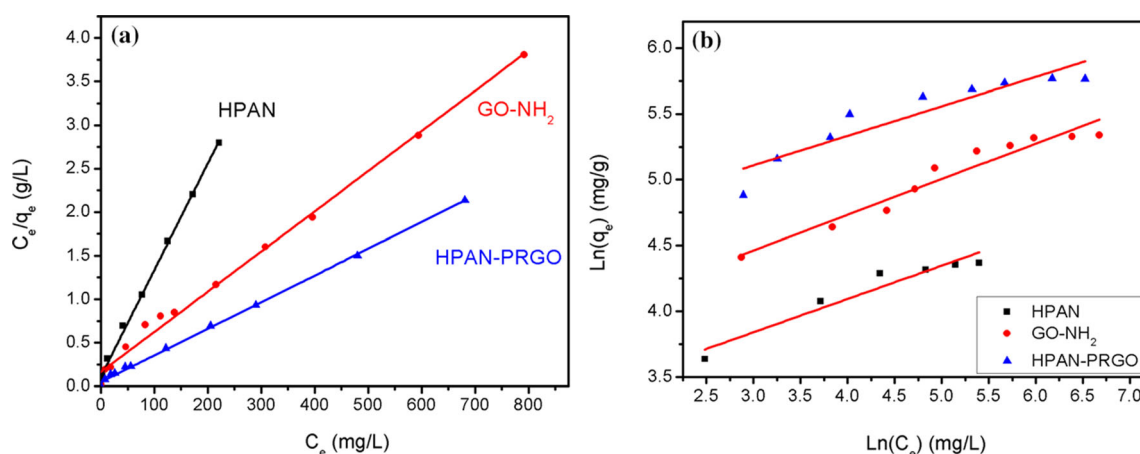


**Figure 8** **a** Langmuir adsorption for the removal of Hg (II) ions using using HPAN, GO-NH<sub>2</sub>, and HPAN-PRGO. **b** Freundlich adsorption for the Hg(II) removal by HPAN, GO-NH<sub>2</sub>, and HPAN-PRGO.

**Table 2** Parameters of Langmuir and Freundlich isotherm models for the removal of Hg (II) ions using HPAN, GO-NH<sub>2</sub>, and HPAN-PRGO

Adsorbent	Langmuir parameters					Freundlich parameters		
	R <sup>2</sup>	b (L/mg)	Q <sub>max, Calc</sub> (mg/g)	Q <sub>Exp</sub> (mg/g)	R <sub>L</sub>	R <sup>2</sup>	K <sub>f</sub>	n
HPAN	0.996	0.108	81.967	97.0	0.029	0.945	21.758	3.952
GO-NH <sub>2</sub>	0.993	0.028	217.391	208.0	0.034	0.935	38.551	3.699
HPAN-PRGO	0.998	0.066	325.732	324.0	0.014	0.844	84.521	4.484

The Langmuir and Freundlich isotherms for the Hg(II) adsorption onto HPAN, GO-NH<sub>2</sub>, and HPAN-PRGO composite are shown in Fig. 8a and b, and the isotherm parameters were presented in Table 2. Based on the correlation coefficient ( $R^2$ ) value, the  $R^2$  obtained from Langmuir isotherm model ( $R^2 > 0.99$ ) was higher than that obtained from Freundlich model HPAN, GO-NH<sub>2</sub>, HPAN-PRGO nanocomposite. Moreover, the dimensionless constant  $R_L$  also falls within the favorable limit between 0 and 1. It was indicated that the Langmuir model was the best-fit model for the Hg(II) adsorption onto adsorbent. Additionally, the  $q_{max}$  values for the adsorption of Hg(II) onto HPAN, GO-NH<sub>2</sub>, HPAN-PRGO nanocomposite as determined from the Langmuir model are 81.967 mg/g, 217.391 mg/g, 325.732 mg/g, respectively, are all the same as the experimental data. The good agreement between the Langmuir adsorption model and the equilibrium data suggests that the extent of Hg(II) ion adsorption is a function of specific binding sites, a limited number of which are located on the sorbent surface. The results of isotherm also indicated that the large number of available amine and carboxylate groups on the

composite surface give rise to the large sorption amount toward Hg(II) [6, 47].

### Adsorption kinetics

The kinetic studies of Hg (II) adsorption onto the HPAN, GO-NH<sub>2</sub>, and HPAN-PRGO composite were performed at 25 °C, and the results are present in Figure 9a. The adsorption amount increased rapidly during the first 15 min and more than 80.0%, 60.2%, 58.6% of the equilibrium adsorption were obtained for HPAN-PRGO, HPAN, and GO-NH<sub>2</sub>, respectively. This means that a large number of vacant adsorption sites on the nanocomposite' surface were available at this stage. Thereafter, the adsorption was fast and the equilibrium was accessed within 90 min. As amount of Hg(II) adsorbed onto the adsorbent increased, the repulsive forces between the adsorbed species are boosted, and adsorption resistance for free metal ions is exacerbated accordingly. The kinetic data were described by using the pseudo-second-order kinetic models and the pseudo-first-order and the details of each model can be shown in the Supporting Information S2.

**For the pseudo-first-order model**, the plot of  $t/q$  versus  $t$  for Hg(II) adsorption onto HPAN, GO-NH<sub>2</sub>,

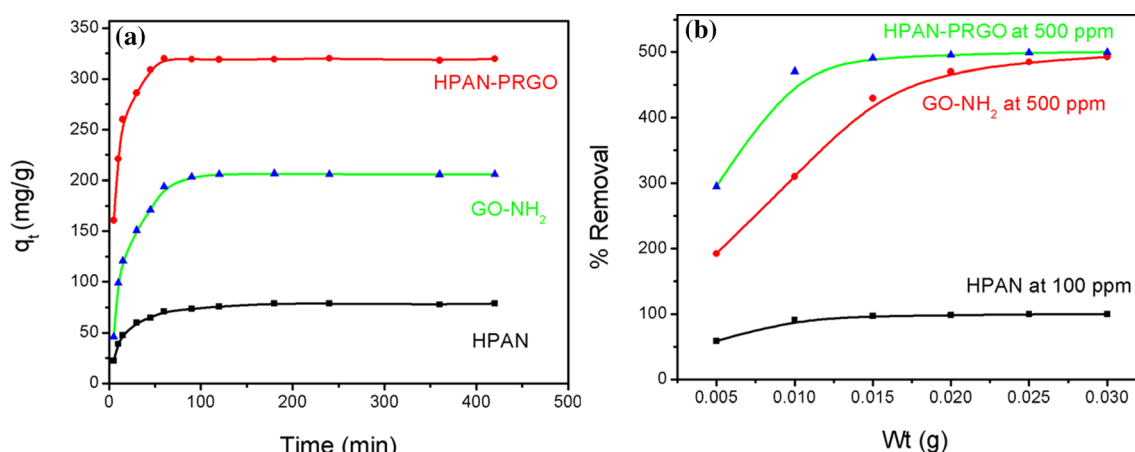


**Figure 9** **a** Effect of contact time on the Hg(II) removal on HPAN, GO-NH<sub>2</sub>, HPAN-PRGO. **b** Effect of adsorbent dose on the Hg(II) removal on HPAN, GO-NH<sub>2</sub>, HPAN-PRGO.



**Table 3** Kinetic parameters for adsorption of 300, 800 ppm Hg (II) ions using HPAN, GO-NH<sub>2</sub>, HPAN-PRGO, respectively

Pseudo-first order	$q_{e \text{ exp.}}$ $\text{mg.g}^{-1}$	$q_{e \text{ cal.}}$ $\text{mg.g}^{-1}$	$K_1$ $\text{min}^{-1}$	$R^2$
HPAN	79.0	5.322	0.0244	0.956
GO-NH <sub>2</sub>	208.0	9.290	0.0379	0.986
HPAN-PRGO	324.0	9.778	0.0625	0.971
Pseudo-second order	$q_{e \text{ exp.}}$ $\text{mg.g}^{-1}$	$q_{e \text{ cal.}}$ $\text{mg.g}^{-1}$	$K_2$ $\text{g. mol}^{-1} \cdot \text{min}^{-1}$	$R^2$
HPAN	79.0	80.906	0.0012	0.999
GO-NH <sub>2</sub>	208.0	212.766	0.0005	0.999
HPAN-PRGO	324.0	321.543	0.0011	0.999

and HPAN-PRGO nanocomposite is shown in Figure S3(B) (Supporting Information) and the parameters of the linear correlation coefficients ( $R^2$ ) and  $K_1$  are calculated and listed in Table 3. It revealed that  $R^2$  are very high. However, there are big differences between the calculated  $q_e$  values ( $q_{e, \text{cal}}$ ) and the experimental  $q_e$  values ( $q_{e, \text{exp}}$ ) which suggested that the pseudo-first-order kinetic model was a poor fit for the adsorption processes of HPAN, GO-NH<sub>2</sub>, and HPAN-PRGO nanocomposite for Hg(II) adsorption [6, 48].

**For the pseudo-second-order model.** Figure S3 (A) (Supporting Information) showed that the pseudo-second-order kinetic model fits well with the practical data (correlation coefficient  $R^2 > 0.999$ ). As seen in Table 3, the calculated maximum uptake capacity of Hg(II) ( $q_{e, \text{max cal.}}$ ) was in good agreement with the practical results. These indicated that the removal processes of Hg(II) onto HPAN, GO-NH<sub>2</sub>, and HPAN-PRGO nanocomposite could be represented by the pseudo-second-order kinetic model. Thus, the mechanism of removal is mainly due to the metal–ligand complex formation between the amine, amide and carboxylate groups of the composite and mercury (II) ions [6, 48].

### Effect of adsorbent dosage

Figure 9b shows the dependence of removal of Hg(II) on dosage of HPAN, GO-NH<sub>2</sub>, HPAN-PRGO nanocomposite. It could be clearly seen that when the sorbent dose increases from 0.005 to 0.03 g, the

adsorption capacity for Hg(II) removals by HPAN, IGO-NH<sub>2</sub>, HPAN-PRGO nanocomposite increased from 59.01 to 99.59 mg/g, from 192.10 to 492.59 mg/g and from 295.06 to 499.99 mg/g, respectively. This can be simply related to accessibility of more sorption sites and the increased sorbent surface area.

### Mechanism of Hg (II) removal

To understand the adsorption mechanism of Hg(II) by HPAN–PRGO nanocomposite nanosheets, the XPS spectra of the composite nanosheets before and after adsorption of Hg(II) ions are given in Fig. 10a–e. Compared to the HPAN–PRGO composite nanosheets before adsorption of Hg(II) ions, two energy peaks at about 105.0 and 100.9 eV corresponding to the binding energies of Hg4f<sub>5/2</sub> and Hg4f<sub>7/2</sub> states are observed after adsorption [28]. This result suggests that Hg(II) was on the HPAN–PRGO composite nanosheets after removal. The intensity of N 1s peak of HPAN–PRGO–Hg greatly decreased and slightly shifted to higher binding energies compared with HPAN–PRGO. This might be attributed to the lone pair of electrons of nitrogen of primary and secondary amine which coordinates with Hg(II) and forms –NH<sub>2</sub>–Hg complex [28, 49]. In addition, Fig. 10c and d show the changes in high-resolution O1s spectra of HPAN/PRGO–NH<sub>2</sub> after and before Hg (II) adsorption. The peaks of O 1s at 528.5 and 530.0 eV, disappeared and the peaks at 533.0 and 531.0 eV significantly increased and shifted to higher binding energies compared with HPAN-PRGO. This is due to the formation of –COO–Hg, O–Hg complexes as shown in Scheme 3.

### Regeneration and recycling

The adsorbent, to be applicable, should have high adsorption capacity and high regeneration ability for recycling use. 2M HCl or 0.017 EDTA is used as desorbing agent for regeneration of the representative sample (HAPN-PRGO) as shown in Table 4, the regenerated adsorbent using HCl as desorbing agent is further treated with NaOH to restore the negative charge of carboxylic group of HPAN–PRGO then washed several times with deionized water. In order to determine the reuse ability of the composites, the successive adsorption–desorption process was carried out for six times at 800 ppm (pH 5.0). Figure 11

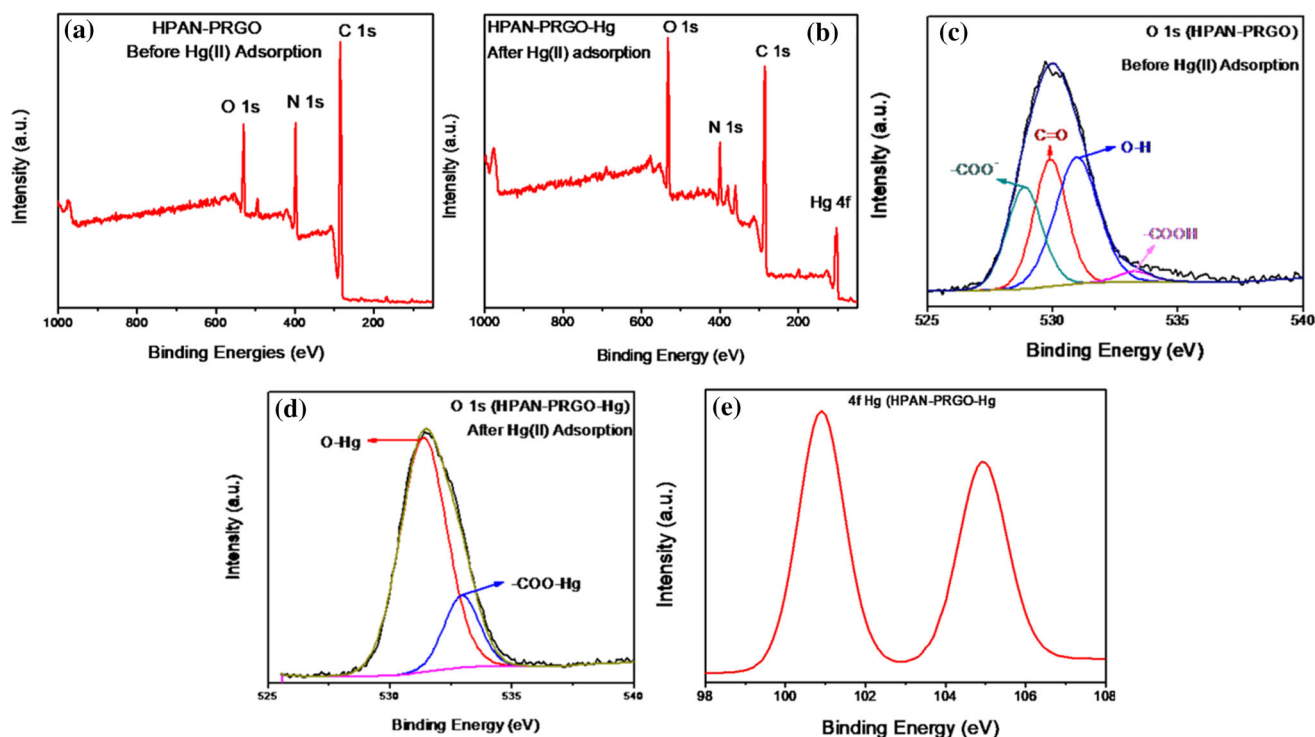
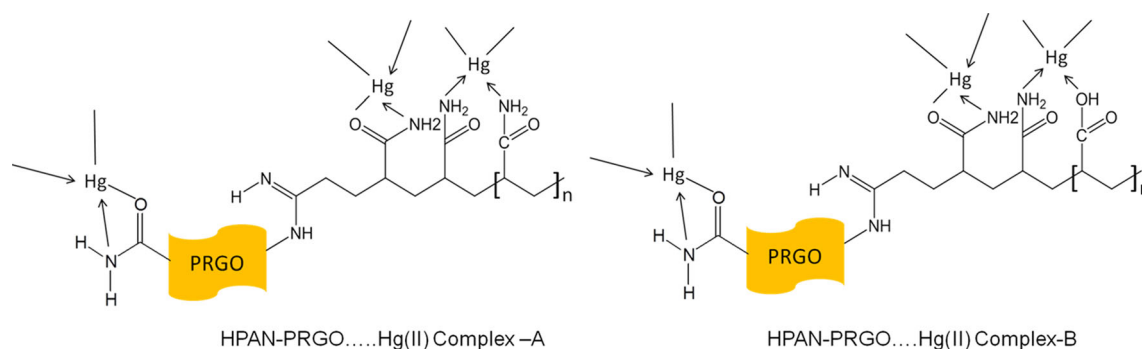


**Figure 10** The XPS survey spectra of HPAN-PRGO **a** before removal of Hg(II) and **b** after removal of Hg(II). The XPS spectra of O1s and Hg4f in HPAN-PRGO before Hg(II) removal **c**, After Hg(II) removal (**d**, **e**).



**Scheme 3** Suggested structures of chelating compounds of Hg(II) ions with HPAN-PRGO.

**Table 4** Desorption studies of mercury from HPAN-PRGO after adsorption of 800 ppm

Eluent	$q_e$ Adsorbed( mg/g )	$q_e$ Desorbed ( mg/g )	% Desorption
0.1 M HCl	320.00	50.99	15.93
0.5 M HCl	320.00	120.96	37.80
1.0 M HCl	320.00	217.00	67.81
2.0 M HCl	320.00	320.0	100.0
0.01 EDTA	320.00	230.00	71.87
0.015EDTA	320.00	300.00	93.75
0.017EDTA	320.00	318.00	99.37

showed that after six adsorption–desorption cycles the reloading efficiency maintained above 90% with no significant loss in adsorption efficiency. Therefore,

HPAN–PRGO composite is an efficient and cost-effective adsorbent for mercury removal from wastewater.

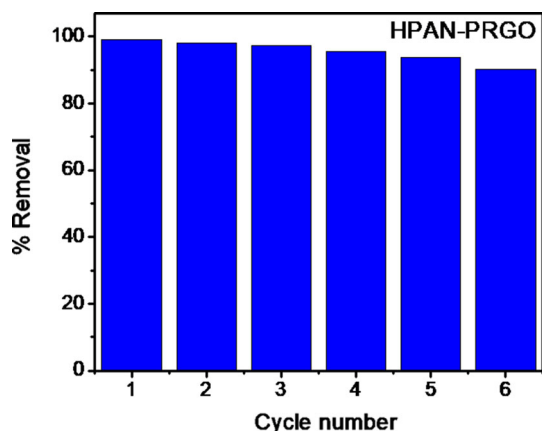


**Figure 11** Recycling of HPAN-PRGO composite for Hg(II) (desorption condition: 0.017 M EDTA), adsorption condition: pH 5, initial concentration of Hg(II) 800 mg/L, dose: 1 g/L).

### Comparison of adsorption capacities

Table 5 describes the comparisons of maximum uptake capacities of HPAN-PRGO nanocomposite prepared in this work with different materials previously reported for Hg(II) adsorption. The HPAN-PRGO nanocomposite has a higher uptake than other adsorbents in the literature. This data clarify strength of HPAN-PRGO nanocomposite in extraction of Hg(II) from polluted water.

**Table 5.** Comparison of the adsorption capacities of Hg(II) ions onto various adsorbents

Adsorbents	Adsorption capacities (mg/g)	Ref.
polymeric magnetic boehmite nanocomposite	36.94	[50]
Polyamine-modified reduced graphene oxide	63.8	[3]
Fe <sub>3</sub> O <sub>4</sub> @SiO <sub>2</sub> @graphene quantum dot core-shell	68.0	[51]
Graphene oxide-based carbon composite	68.8	[52]
polythiophene/graphene oxide nanocomposite	113.6	[53]
Novel muscovite/zeolite aluminosilicate composite	117.0	[54]
magnetic carbon nanotubes	172.8	[55]
silica/polyacrylamide composite	177.0	[56]
Thiol-/thioether-functionalized porous organic polymers	180.0	[57]
3D reduced graphene oxide aerogel	185.0	[58]
Glutamine modified chitosan magnetic composite	199.2	[59]
Polyacrylamidoxime chelating fiber	222.27	[60]
Imino diacetic acid improved graphene oxide (Imino-IGO)	230.0	[20]
Thiol modified porous polyaminal-networked polymer	312.0	[17]
Thio-functionalized polyacrylonitrile Fiber	322.8	[39]
Thio-functionalized polyacrylonitrile (PAN) fiber	357.0	[5]
2-Imino-4-thiobiuret-partially reduced graphene oxide (IT-PRGO)	624.0	[19]
HPAN-PRGO	324.0	This study

### Conclusion

In this work, PAN nanoparticles grafted on the aminated partially reduced graphene oxide nanosheets were synthesized and characterized for the effective extraction of Hg(II) ions from polluted water. FTIR, XRD, Raman spectra, TEM, SEM, and XPS measurements indicated that the PAN nanoparticles were successfully bonded to the free amino groups on the functionalized graphene nanosheets. The pH had a strong influence on the adsorption behavior of the material and pH 5 is the optimal pH. The adsorption was found to increase with increasing contact time and initial metal concentration with maximum uptake capacity of 324.0 mg/g and equilibrium time 90 min. XPS analysis approved that the Hg(II) removal from polluted water was due to the coordination between nitrogen containing functional groups on the surface of the composite and the Hg(II) ions. The adsorption of Hg(II) was described well with Langmuir isotherm model and pseudo-second-order kinetic model and maximal adsorption being 324.0 mg/g. The regeneration experiments showed that submersion of the HPAN-PRGO loaded with Hg(II) in 10 mL of 2.0 M HCl or 0.017 M EDTA resulted in the desorption of more than 99.0% of the

adsorbed amount of the Hg(II) and the HPAN–PRGO showed a good stability within six cycles. The obtained results suggested that the HPAN–PRGO has a superior capacity for Hg(II) ions removal from wastewater effluents.

## Acknowledgments

We thank the National Science Foundation (CHE-1900094) for the partial support of this work.

## Compliance with ethical standards

**Conflict of interest** There are no conflicts to declare.

**Supplementary Information:** The online version contains supplementary material available at (<http://doi.org/10.1007/s10853-021-05797-2>)

## References

- [1] Kampalananwat P, Supaphol P (2010) Preparation and adsorption behavior of aminated electrospun polyacrylonitrile nanofiber mats for heavy metal ion removal. *ACS Appl Mater Interfaces* 2:3619–3627
- [2] Sun Q, Aguila B, Perman J et al (2017) Postsynthetically modified covalent organic frameworks for efficient and effective mercury removal. *J Am Chem Soc* 139:2786–2793
- [3] Yap PL, Tung TT, Kabiri S, Matulick N, Tran DN, Losic D (2020) Polyamine-modified reduced graphene oxide: a new and cost-effective adsorbent for efficient removal of mercury in waters. *Sep Purif Technol* 238:116441
- [4] Y Yu, G Li, J Liu, D Yuan (2020) A recyclable fluorescent covalent organic framework for exclusive detection and removal of mercury (II). *Chem Eng J* 401:126139
- [5] Deng S, Yu C, Liu X et al (2020) Efficient and enhanced Hg<sup>2+</sup> removal from water using a thio functionalized fibrous adsorbent prepared with microwave irradiation Batch and fixed-bed column study. *J Clean Prod* 267:122163
- [6] Kabiri S, Tran DN, Azari S, Losic D (2015) Graphene-diatom silica aerogels for efficient removal of mercury ions from water. *ACS Appl Mater & Interfaces* 7:11815–11823
- [7] Wang X, Lv P, Zou H, Li Y, Li X, Liao Y (2016) Synthesis of poly (2-aminothiazole) for selective removal of Hg (II) in aqueous solutions. *Ind Eng Chem Res* 55:4911–4918
- [8] Cui W-R, Zhang C-R, Jiang W et al (2019) Covalent organic framework nanosheet-based ultrasensitive and selective colorimetric sensor for trace Hg<sup>2+</sup> detection. *ACS Sustain Chem Eng* 7:9408–9415
- [9] Afshari M, Dinari M, Zargoosh K, Moradi H (2020) Novel triazine-based covalent organic framework as a superadsorbent for the removal of mercury (II) from aqueous solutions. *Ind Eng Chem Res* 59:9116–9126
- [10] Liu L, Ding L, Wu X, Deng F, Kang R, Luo X (2016) Enhancing the Hg (II) removal efficiency from real wastewater by novel thymine-grafted reduced graphene oxide complexes. *Ind Eng Chem Res* 55:6845–6853
- [11] Navarro RR, Wada S, Tatsumi K (2005) Heavy metal precipitation by polycation–polyanion complex of PEI and its phosphonomethylated derivative. *J Hazard Mater* 123:203–209
- [12] Chen K, Zhang Z, Xia K, Zhou X, Guo Y, Huang T (2019) Facile synthesis of thiol-functionalized magnetic activated carbon and application for the removal of mercury (II) from aqueous solution. *ACS Omega* 4:8568–8579
- [13] Deb AS, Dwivedi V, Dasgupta K, Ali SM, Shenoy K (2017) Novel amidoamine functionalized multi-walled carbon nanotubes for removal of mercury (II) ions from wastewater: combined experimental and density functional theoretical approach. *Chem Eng J* 313:899–911
- [14] Das S, Chatterjee S, Mondal S et al (2020) Thiadiazole containing N-and S-rich highly ordered periodic mesoporous organosilica for efficient removal of Hg (ii) from polluted water. *Chem Commun* 56:3963–3966
- [15] Wang L, Wang M, Li Z, Gong Y (2020) Enhanced removal of trace mercury from surface water using a novel Mg<sub>2</sub>Al layered double hydroxide supported iron sulfide composite. *Chem Eng J* 393:124635–124647
- [16] Y Li, T Hu, R Chen, et al (2020) Novel thiol-functionalized covalent organic framework as adsorbent for simultaneous removal of BTEX and mercury (II) from water. *Chem Eng J* 398:125566
- [17] Ryu J, Lee MY, Song MG, Baeck S-H, Shim SE, Qian Y (2020) Highly selective removal of Hg (II) ions from aqueous solution using thiol-modified porous polyaminal-networked polymer. *Sep Purif Technol* 250:117120–117130
- [18] Mohammadnia E, Hadavifar M, Veisi H (2019) Kinetics and thermodynamics of mercury adsorption onto thiolated graphene oxide nanoparticles. *Polyhedron* 173:114139–114147
- [19] Awad FS, AbouZeid KM, El-Maaty WMA, El-Wakil AM, El-Shall MS (2017) Efficient removal of heavy metals from polluted water with high selectivity for mercury (II) by 2-imino-4-thiobiuret–partially reduced graphene oxide (IT-PRGO). *ACS Appl Mater Interfaces* 9:34230–34242
- [20] Awad FS, AbouZied KM, Abou El-Maaty WM, El-Wakil AM, El-Shall MS (2020) Effective removal of mercury (II) from aqueous solutions by chemically modified graphene oxide nanosheets. *Arab J Chem* 13:2659–2670



- [21] Shirzadi H, Nezamzadeh-Ejhi A (2017) An efficient modified zeolite for simultaneous removal of Pb (II) and Hg (II) from aqueous solution. *J Mole Liq* 230:221–229
- [22] Ganguly M, Tao Y, Lee B, Ariya PA (2020) Natural kaolin: sustainable technology for the instantaneous and energy-neutral recycling of anthropogenic mercury emissions. *ChemSusChem* 13:165–172
- [23] Kirupha SD, Kalaivani S, Vidhyadevi T et al (2016) Effective removal of heavy metal ions from aqueous solutions using a new chelating resin poly [2, 5-(1, 3, 4-thiadiazole)-benzalimine]: kinetic and thermodynamic study. *J Water Reuse Desalin* 6:310
- [24] Deng S, Bai R, Chen JP (2003) Aminated polyacrylonitrile fibers for lead and copper removal. *Langmuir* 19:5058–5064
- [25] Ma N, Yang Y, Chen S, Zhang Q (2009) Preparation of amine group-containing chelating fiber for thorough removal of mercury ions. *J Hazard Mater* 171:288–293
- [26] Cai X, Lin M, Tan S et al (2012) The use of polyethyleneimine-modified reduced graphene oxide as a substrate for silver nanoparticles to produce a material with lower cytotoxicity and long-term antibacterial activity. *Carbon* 50:3407–3415
- [27] Yang Y, Xie Y, Pang L et al (2013) Preparation of reduced graphene oxide/poly (acrylamide) nanocomposite and its adsorption of Pb (II) and methylene blue. *Langmuir* 29:10727–10736
- [28] Chandra V, Kim KS (2011) Highly selective adsorption of  $Hg^{2+}$  by a polypyrrole–reduced graphene oxide composite. *Chem Commun* 47:3942–3944
- [29] Lu A, Kiefer A, Schmidt W, Schüth F (2004) Synthesis of polyacrylonitrile-based ordered mesoporous carbon with tunable pore structures. *Chem Mater* 16:100–103
- [30] Pekel N, Şahiner N, Güven O (2001) Use of amidoximated acrylonitrile/N-vinyl 2-pyrrolidone interpenetrating polymer networks for uranyl ion adsorption from aqueous systems. *J Appl Polym Sci* 81:2324–2329
- [31] Marcano DC, Kosynkin DV, Berlin JM et al (2010) Improved synthesis of graphene oxide. *ACS Nano* 4:4806–4814
- [32] Zhang Y, Zhuang X, Gu W, Zhao J (2015) Synthesis of polyacrylonitrile nanoparticles at high monomer concentrations by AIBN-initiated semi-continuous emulsion polymerization method. *Eur Polym J* 67:57–65
- [33] Lee I, Kim S, S-n Kim Y, Jang J Jang (2014) Highly fluorescent amidine/schiff base dual-modified polyacrylonitrile nanoparticles for selective and sensitive detection of copper ions in living cells. *ACS Appl Mater Interfaces* 6:17151–17156
- [34] Deng S, Wang P, Zhang G, Dou Y (2016) Polyacrylonitrile-based fiber modified with thiosemicarbazide by microwave irradiation and its adsorption behavior for Cd (II) and Pb (II). *J Hazard Mater* 307:64–72
- [35] Li G, Xiao J, Zhang W (2012) Efficient and reusable amine-functionalized polyacrylonitrile fiber catalysts for Knoevenagel condensation in water. *Green Chem* 14:2234–2242
- [36] Kampalanonwat P, Supaphol P (2011) Preparation of hydrolyzed electrospun polyacrylonitrile fiber mats as chelating substrates: a case study on copper (II) ions. *Ind Eng Chem Res* 50:11912–11921
- [37] Abdelsayed V, Moussa S, Hassan HM, Aluri HS, Collinson MM, El-Shall MS (2010) Photothermal deoxygenation of graphite oxide with laser excitation in solution and graphene-aided increase in water temperature. *J Phys Chem Lett* 1:2804–2809
- [38] Bobb JA, Awad FS, Moussa S, El-Shall MS (2020) Laser synthesis of magnetite-partially reduced graphene oxide nanocomposites for arsenate removal from water. *J Mater Sci* 55:5351–5363. <https://doi.org/10.1007/s10853-020-04363-6>
- [39] Deng S, Zhang G, Liang S, Wang P (2017) Microwave assisted preparation of thio-functionalized polyacrylonitrile fiber for the selective and enhanced adsorption of mercury and cadmium from water. *ACS Sustain Chem Eng* 5:6054–6063
- [40] Singh SK, Singh MK, Kulkarni PP, Sonkar VK, Grácio JJ, Dash D (2012) Amine-modified graphene: thrombo-protective safer alternative to graphene oxide for biomedical applications. *ACS Nano* 6:2731–2740
- [41] Uddin ME, Layek RK, Kim NH, Hui D, Lee JH (2015) Preparation and properties of reduced graphene oxide/polyacrylonitrile nanocomposites using polyvinyl phenol. *Compos Part B: Eng* 80:238–245
- [42] Sreeprasad T, Maliyekkal SM, Lisha K, Pradeep T (2011) Reduced graphene oxide–metal/metal oxide composites: facile synthesis and application in water purification. *J Hazard Mater* 186:921–931
- [43] Chiang Y-C, Lee C-Y, Lee H-C (2007) Surface chemistry of polyacrylonitrile-and rayon-based activated carbon fibers after post-heat treatment. *Mater Chem Phys* 101:199–210
- [44] Zhu B, Xia P, Ho W, Yu J (2015) Isoelectric point and adsorption activity of porous g-C<sub>3</sub>N<sub>4</sub>. *Appl Surf Sci* 344:188–195
- [45] Park SS, Chu S-W, Xue C, Zhao D, Ha C-S (2011) Facile synthesis of mesoporous carbon nitrides using the incipient wetness method and the application as hydrogen adsorbent. *J Mater Chem* 21:10801–10807
- [46] Wang J, Qin W, Liu X, Liu H (2013) Synthesis and characterization of hydroxyapatite on hydrolyzed polyacrylonitrile nanofiber templates. *RSC Adv* 3:11132–11139
- [47] Xiong C, Jia Q, Chen X, Wang G, Yao C (2013) Optimization of polyacrylonitrile-2-aminothiazole resin

- synthesis, characterization, and its adsorption performance and mechanism for removal of Hg (II) from aqueous solutions. *Ind Eng Chem Res* 52:4978–4986
- [48] Pourbeyram S (2016) Effective removal of heavy metals from aqueous solutions by graphene oxide–zirconium phosphate (GO–Zr-P) nanocomposite. *Ind Eng Chem Res* 55:5608–5617
- [49] Kumar ASK, Jiang S-J (2015) Preparation and characterization of exfoliated graphene oxide–L-cystine as an effective adsorbent of Hg (II) adsorption. *RSC Adv* 5:6294–6304
- [50] H Alinezhad, M Zabihi, D Kahfroushan (2020) Design and fabrication the novel polymeric magnetic boehmite nanocomposite (boehmite@ Fe<sub>3</sub>O<sub>4</sub>@ PLA@ SiO<sub>2</sub>) for the remarkable competitive adsorption of methylene blue and mercury ions. *J Phys Chem Solids* 144:109515
- [51] Alvand M, Shemirani F (2017) A Fe<sub>3</sub>O<sub>4</sub>@ SiO<sub>2</sub>@ graphene quantum dot core-shell structured nanomaterial as a fluorescent probe and for magnetic removal of mercury (II) ion. *Microchimica Acta* 184:1621–1629
- [52] Esfandiyari T, Nasirizadeh N, Dehghani M, Ehrampoosh MH (2017) Graphene oxide based carbon composite as adsorbent for Hg removal: preparation, characterization, kinetics and isotherms studies. *Chin J Chem Eng* 25:1170–1175
- [53] Muliwa AM, Onyango MS, Maity A, Ochieng A (2017) Batch equilibrium and kinetics of mercury removal from aqueous solutions using polythiophene/graphene oxide nanocomposite. *Water Sci Technol* 75:2841–2851
- [54] Salam MA, Abukhadra MR, Mostafa M (2020) Effective decontamination of As (V), Hg (II), and U (VI) toxic ions from water using novel muscovite/zeolite aluminosilicate composite: adsorption behavior and mechanism. *Environ Sci Pollut Res* 27:13247–13260
- [55] Homayoon F, Faghihian H, Torki F (2017) Application of a novel magnetic carbon nanotube adsorbent for removal of mercury from aqueous solutions. *Environ Sci Pollut Res* 24:11764–11778
- [56] Saad A, Bakas I, Piquemal J-Y, Nowak S, Abderrabba M, Chehimi MM (2016) Mesoporous silica/polyacrylamide composite: preparation by UV-graft photopolymerization, characterization and use as Hg (II) adsorbent. *Appl Surf Sci* 367:181–189
- [57] Cheng J, Li Y, Li L, Lu P, Wang Q, He C (2019) Thiol-/thioether-functionalized porous organic polymers for simultaneous removal of mercury (II) ion and aromatic pollutants in water. *New J Chem* 43:7683–7693
- [58] Wu S, Kong L, Liu J (2016) Removal of mercury and fluoride from aqueous solutions by three-dimensional reduced-graphene oxide aerogel. *Res Chem Intermed* 42:4513–4530
- [59] Tao X, Li K, Yan H, Yang H, Li A (2016) Simultaneous removal of acid green 25 and mercury ions from aqueous solutions using glutamine modified chitosan magnetic composite microspheres. *Environ Pollut* 209:21–29
- [60] Bilba D, Bilba N, Moroi G (2007) Removal of mercury (II) ions from aqueous solutions by the polyacrylamidoxime chelating fiber. *Sep Sci Technol* 42:171–184

**Publisher's Note** Springer Nature remains neutral with regard to jurisdictional claims in published maps and institutional affiliations.